ENGINEERING TRANSACTIONS • *Engng. Trans.* • **43**, 1–2, 327–355, 1995
Polish Academy of Sciences • Institute of Fundamental Technological Research

THE 18G2A STEEL (CONSTRUCTION STEEL) CYCLIC BEHAVIOUR IN THE CASE OF COMPLEX UNIAXIAL LOADING (*)

E. SENDER and W. TRĄMPCZYŃSKI (WARSZAWA)

This paper is concerned with the phenomenon of uniaxial cyclic material behaviour in the plastic range. A set of systematic strain and stress-controlled cyclic (tension – compression) experiments was conducted on round bar specimens made of 18G2A (heat treated) construction steel at room temperature. Results concerning monotonic loading, strain-controlled symmetric cyclic loading and stress-controlled non-symmetric cyclic loading (ratchetting) are presented and summarized. All experiments were performed on similar specimens, the same laboratory equipment and using the same experimental technique. The technique of successive unloadings (proposed by the author [1, 2]) was used to obtain some additional information concerning the yield surface position and its evolution for the loading programs mentioned above.

1. Introduction

In various engineering problems, the structures and structural components must be designed to withstand cyclic loads that can lead to occasional extrusions into the plastic range of the material behaviour. Structures located in earthquake areas, various nuclear reactor components, offshore structures and many structural components operating at elevated temperatures can be listed as the examples. Hence it is quite important to collect wide range of data concerning material behavior for different plastic loading histories, including cyclic symmetric and non-symmetric loading. Such data can then be used as a necessary tool for the prediction of the allowable number of load cycles such structures can sustain, or as a useful database for constitutive model testing and creation of new models.

Although quite a lot of experimental programs (both for uniaxial and for multiaxial loading) in this field were carried out since quite a long time [3 – 11] and several plasticity theories were proposed [20 – 27], there is still lack of consistent data (even uniaxial) obtained using this same equipment, specimens and experimental technique.

(*) Paper presented at 30th Polish Solid Mechanics Conference, Zakopane, September 5 – 9, 1994.

It concerns also the evolution of the yield surface due to complex plastic histories, what is quite important since majority of the proposed theories are based on the idea of kinematic and isotropic hardening.

In this paper, the results concerning uniaxial monotonic loading and cyclic loading, with special emphasis on stress-controlled non-symmetric cyclic loading (ratchetting) are presented, and following phenomena are described:

- the evolution of kinematic and isotropic hardening for monotonic and cyclic loading,
- memory of maximal prestress (cyclic and monotonic one),
- the map of material behaviour showing elastic, shake-down and ratchetting zones,
- relation between mean stress and amplitude to describe the ratchetting strain rate in the steady state.

All experiments were performed on the same specimens (round bar made of 18G2A Steel), laboratory equipment and using the same experimental technique.

For a better comparison with the existing theories, results concerning the yield surface parameters evolution, obtained by the two-point unloading technique [1, 2], are also presented. This technique enables us to get some additional information on the yield surface evolution, when only two well defined points of that surface are known.

Let us assume [1] the basic program 0-C of plastic straining [Fig. 1a]. The loading is interrupted at point A (S_{ij}) where the specimen is unloaded and then reloaded into reverse straining direction until the small value of the plastic strain increment of $\eta = e_e^p$ (the yield definition) is achieved (Fig. 1b). The end of the stress deviator S_{ij}^R lies on the yield surface at point B', where the plastic strain-rate vector has the direction opposite to that prescribed in the basic program. In this moment the reloading process is stopped, the specimen is unloaded and loaded in the former direction. The basic straining program is then continued. In this way two well defined points S_{ij} and S_{ij}^R on the current yield surface are obtained, for the chosen plastic strain history (it is assumed that the plastic strain increment due to point B' identification is negligible). The first point lies on the yield surface where the plastic strain rate vector has the direction prescribed by the basic program, and the second one lies on the yield surface where the plastic strain rate vector has the opposite direction.

Due to simplicity of this technique and in view of the fact that it is only one yield surface "punch", it can be used several times during the whole loading history. Even for quite complicated loadings (e.g. cyclic ones), the

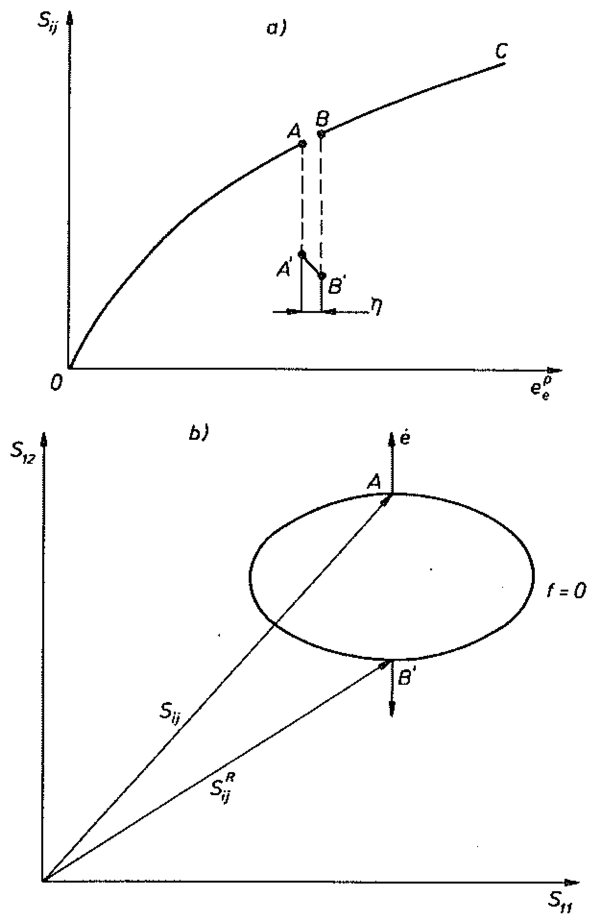

FIG. 1. Theoretical basis for the two yield points technique.

evolution of such parameters as

$$(1) \qquad Y_{ij} = (S_{ij} - S_{ij}^R)/2, \qquad \pi_{ij} = (S_{ij} + S_{ij}^R)/2$$

can be followed this way and used for experimental comparison of theoretical predictions.

Assuming that the current yield surface can be approximated by the Huber-Mises spheres it is possible to show that

$$(2) \qquad Y_{ij} = (S_{ij} - S_{ij}^R)/2 = n_{ij}R(H), \qquad \pi_{ij} = (S_{ij} + S_{ij}^R)/2 = \alpha_{ij}\,.$$

Hence, in such a case one can experimentally determine not only the evolution of Y_{ij} and π_{ij}, but also the evolution of the yield surface radius (R) and the position (α_{ij}) of its center. In the case of uniaxial loading the yield radius $Y_1(R)$ and its position π_i can be easily calculated. The technique mentioned above was successfully used even in the case of quite complicated monotonic and cyclic (strain-controlled) symmetric loading [28].

2. Experimental procedure

The experimental programs were performed on solid circular specimens made of 18G2A steel at room temperature. The specimen dimensions: diameter $D = 12$ m, specimen gauge length $L = 15$ mm were chosen experimentally and then confirmed theoretically using the final element program ABAQUS. Tension-compression cyclic programs were conducted in a closed-loop servo-hydraulic Instron 8501 uniaxial machine with an axial load capacity ±100 kN. The facility provides the capability of testing under load, displacement, or strain control. The load was measured by a calibrated load cell, and the strain was monitored by 10 mm gauge extensometer. Force acting on the specimen and its elongation were read by a computer (HP Vectra), then elaborated and the results obtained were used for continuous machine con-

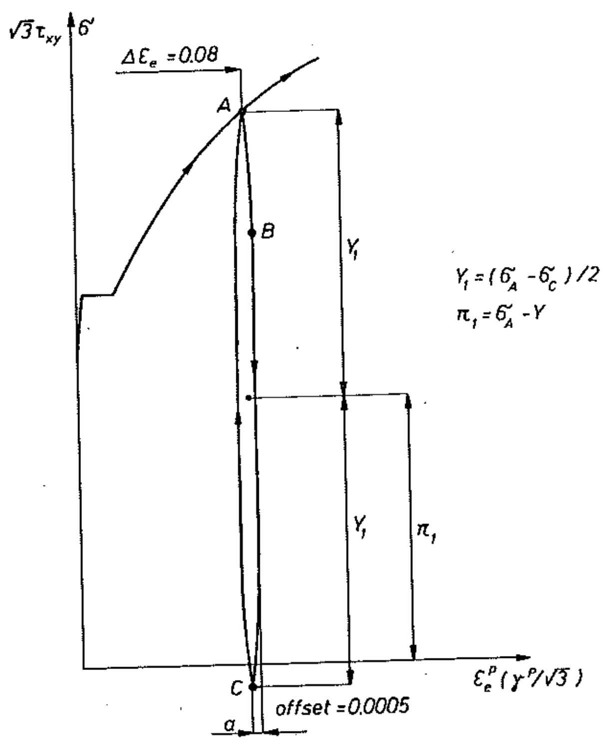

FIG. 2. Application of the "two-point" technique in the case of monotonic tension.

trol. The longest time of information path: machine-computer-machine of the program used was 0.05 s. All programs were performed with a constant plastic strain rate $\dot{\varepsilon}_x^p = 3.4 \times 10^{-4}\text{s}^{-1}$ and the actual stress versus the logarithmic plastic strain were calculated and plotted ($\varepsilon_x = \ln(l/l_0)$, $\sigma = P/F_a$, where l_0 – gauge length, F_a – current specimen cross-section, P – force). The yield points were defined by the offset definition $\eta = 0.0005$ (Fig. 2) in the following way: at a chosen moment of plastic strain history the stress value σ_A was recorded, the straining direction was reversed and the slope of the unloading curve was measured. At point B this slope was equal to Young's modulus for the virgin material and the straight line "a" of the same slope was determined. The distance between the successive points on the unloading curve (loading in "opposite" direction) and on this straight line was then calculated. When it was equal to the value η (the "offset definition"), the second yield point σ_C was found and the strain direction was changed to the former one. Then the values $\pi_1 = (\sigma_A + \sigma_C)/2$ and $Y_1 = (\sigma_A - \sigma_C)/2$ were calculated and recorded. As it was mentioned above, in the case of Huber – Mises yield surface, π_1 and Y_1 parameters denote respectively the yield surface center position and its radius.

3. Experimental results

Although the experimental results, for monotonic and cyclic strain-controlled programs, show the same effects and look similar to those presented in [1, 28], they were obtained for a similar material but using the round bar uniaxial specimens under tension-compression. They are presented to complete the results and compare with the results obtained for cyclic stress-controlled loading (ratchetting).

a. Monotonic tension (with unloadings)

The specimen was loaded by tension at the constant plastic strain rate $\dot{\varepsilon}_x^p = 3.4 \times 10^{-4}\,\text{s}^{-1}$. After every chosen plastic strain increment $\Delta\varepsilon_x^p$ the π_1 and Y_1 values were determined in the way described above. The loading paths for stress σ, π_1 and Y_1 are shown in Fig. 3. The parameter Y_1 saturates at plastic strains $\varepsilon_x^p \approx 0.1$ and further material hardening is caused by increasing π_1 value only. The yield knee AB (Fig. 3a and Fig. 3b) is formed as a result of two simultaneous processes: increase of parameter π_1 and decrease of parameter Y_1.

a)

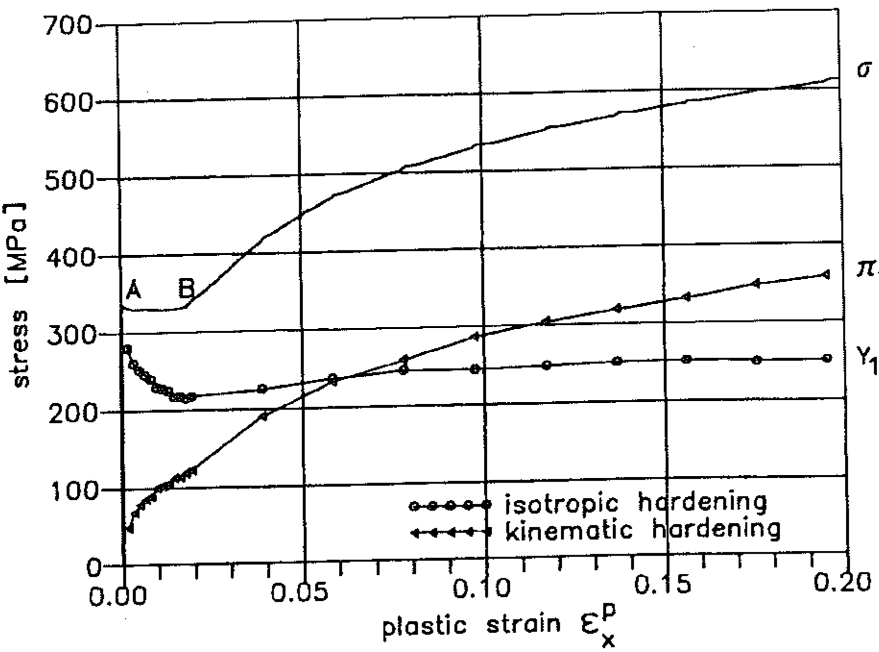

b)

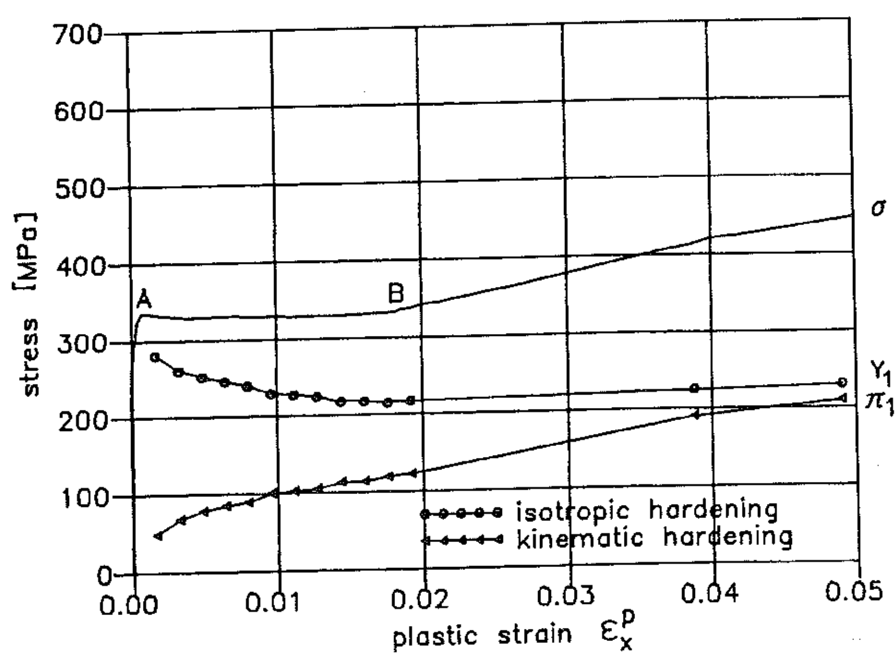

FIG. 3. Monotonic tension (with unloadings), Δ – π_1 evolution (kinematic hardening), o – Y_1 evolution (isotropic hardening).

b. Strain-controlled cyclic tension-compression (with unloadings)

In Fig. 4 a typical stress-strain curve is shown for a virgin material under cyclic tension-compression loading with constant strain amplitude ($\varepsilon_x^p = \pm 0.02$). Using the "unloading technique", it was possible to determine the variation of parameters π_1 (Fig. 4a) and Y_1 (Fig. 4b) from the beginning up to the stabilized loop. Solid line shows the first three half-cycles, and the dashed one shows the stabilized loop. The material exhibits cyclic hardening, the major part of which occurs during the first three half-cycles (both for π_1 and for Y_1). The general shape of the π_1 path changes during the first three half-cycles, and then remains almost constant up to the steady state being similar to the stress-strain curve. In the steady state cycles parameter Y_1 remains constant ($Y_1 = \text{const}$).

In Fig. 5 a typical stress-strain curve is shown for cyclic tension-compression loading with constant strain amplitude ($\varepsilon_x^p = \pm 0.005$), but for the material prestrained by cyclic loading with a higher strain amplitude ($\varepsilon_x^p = \pm 0.02$). The evolution of π_1 and Y_1 from the moment of the amplitude change up to the stabilized loop is presented in a way similar to that in Fig. 4. Solid line shows the first three half-cycles, and the dashed one shows the stabilized loop. Material exhibits cyclic softening, major part of which occurs during the first three half-cycles (both for π_1 and for Y_1). The general shape of the π_1 path changes during the first three half-cycles, and than remains almost constant up to the steady state. In the steady state cycles parameter Y_1 remains constant.

In Fig. 6 the skeleton curves for stress σ (Fig. 6a), π_1 (Fig. 6b) and Y_1 (Fig. 6c) in the case of increasing strain amplitudes $\varepsilon_x^p = \pm 0.005, 0.01, 0.015, 0.02$ (solid line) are compared with those for decreasing strain amplitudes from $\varepsilon_x^p = \pm 0.02$ to $\varepsilon_x^p = \pm 0.005$ (dashed line). The proper monotonic tension curves for stress, π_1 and Y_1, are also shown for comparison. The values of π_1 and Y_1 for cyclic amplitude $\varepsilon_x^p = \pm 0.02$ for a virgin material are the same as for material with the history of increasing amplitudes. It means that cyclic loading history with smaller amplitudes has no influence on the material cyclic behaviour with higher amplitudes. Difference between the solid and dashed lines indicates the influence of the cyclic loading history with higher amplitudes on the material behaviour under cyclic loading with smaller amplitudes. Such memory of maximal prestress is included mainly in behaviour of the π_1 parameter. Almost no influence on the values of Y_1 was observed.

The stress-strain, π_1 and Y_1 cyclic curves for the specimen plastically prestrained up to $\varepsilon_x^p = 0.092$ and then cyclically loaded with plastic strain

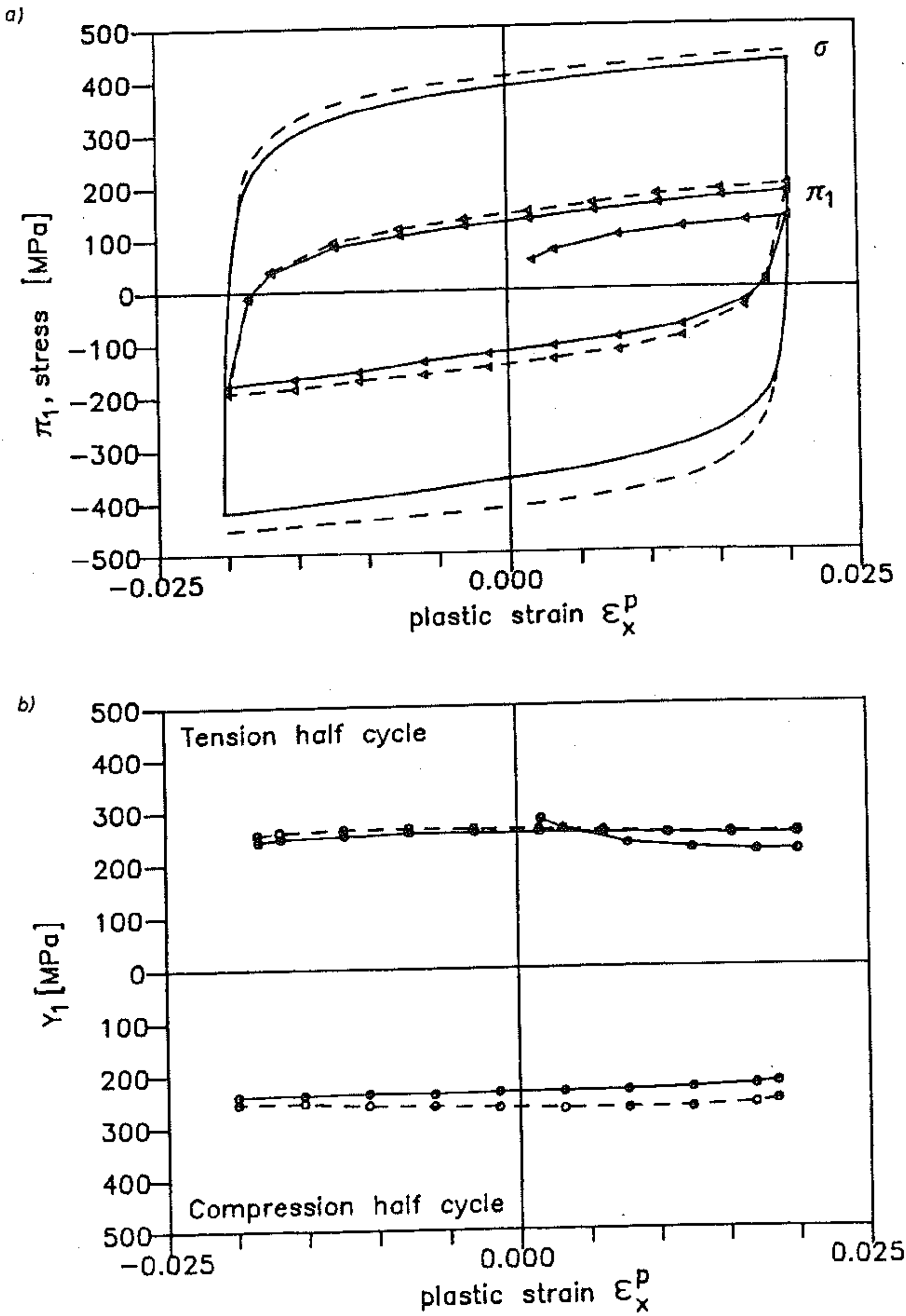

FIG. 4. Cyclic tension-compression loading with $\varepsilon_x^p = \pm 0.02$ strain amplitude, $\Delta - \pi_1$ evolution (kinematic hardening), $\circ - Y_1$ evolution (isotropic hardening).

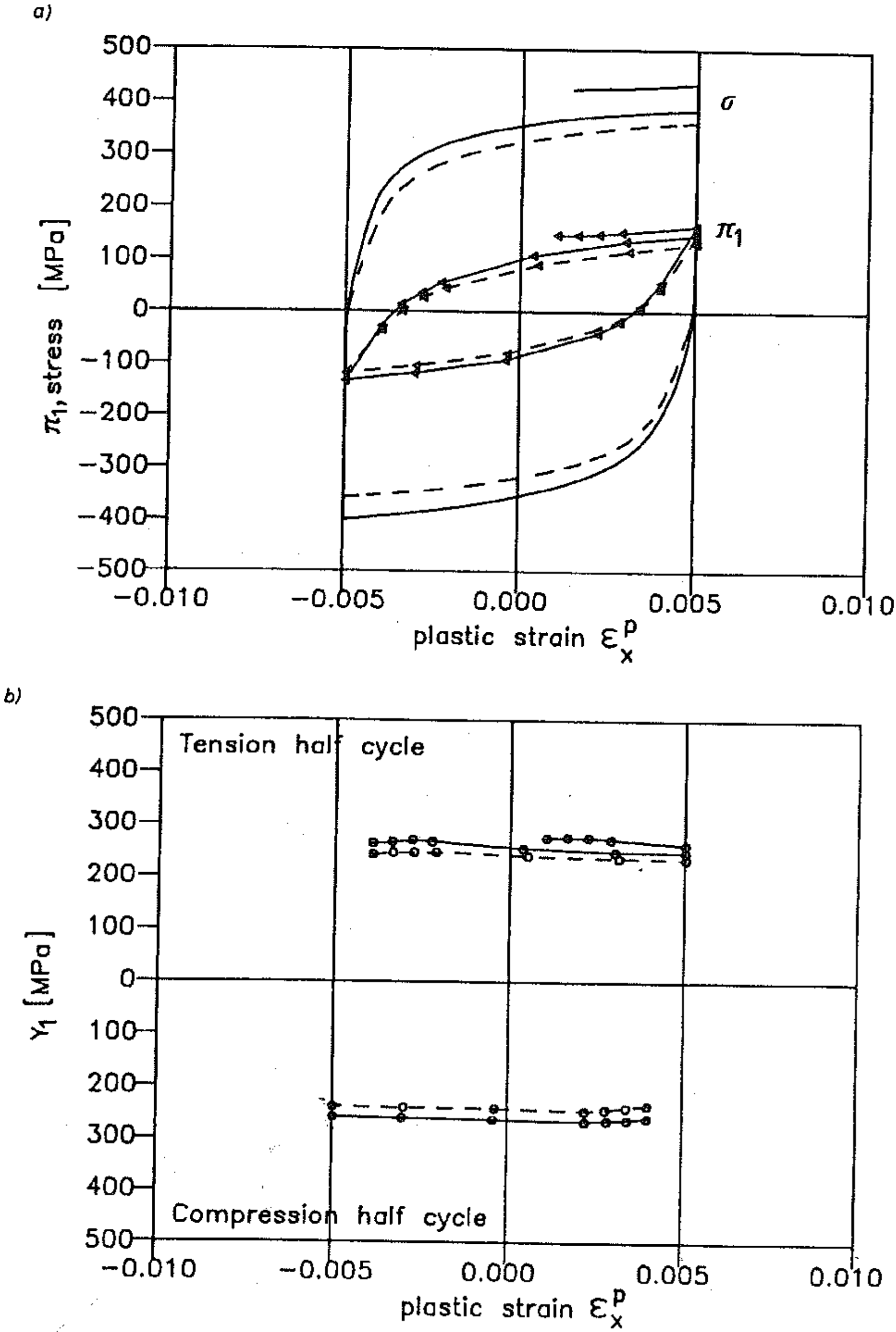

FIG. 5. Cyclic tension-compression loading with $\varepsilon_x^p = \pm 0.005$ strain amplitude after cyclic loading with $\varepsilon_x^p = \pm 0.02$, Δ – π_1 evolution (kinematic hardening), o – Y_1 evolution (isotropic hardening).

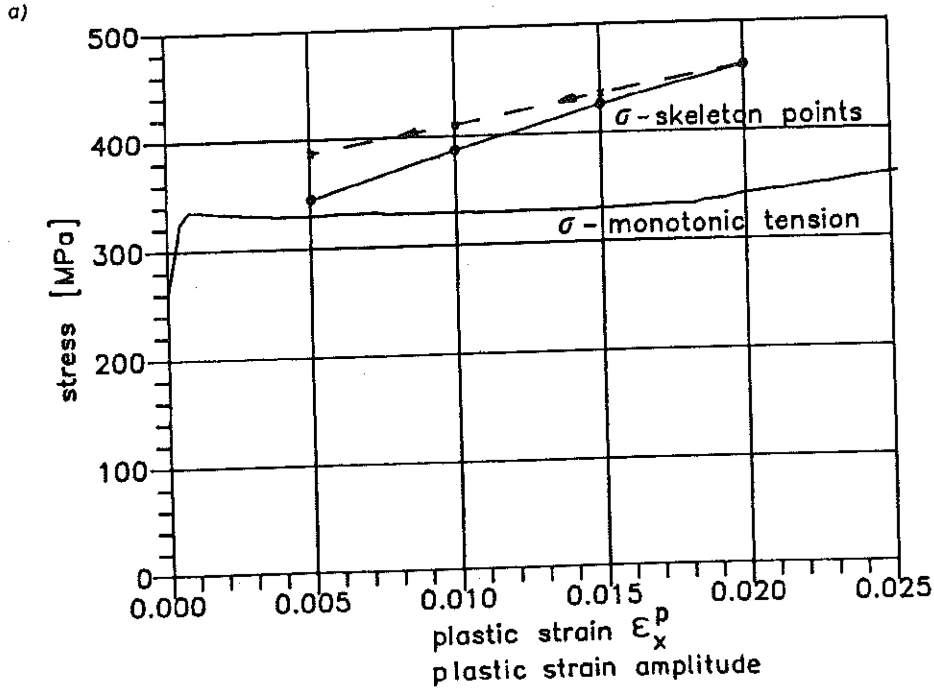
a)
500
400
300
200
100
0
stress [MPa]
σ - skeleton points
σ - monotonic tension
0.000
0.005
0.010
0.015
0.020
0.025
plastic strain ε$_x^p$
plastic strain amplitude

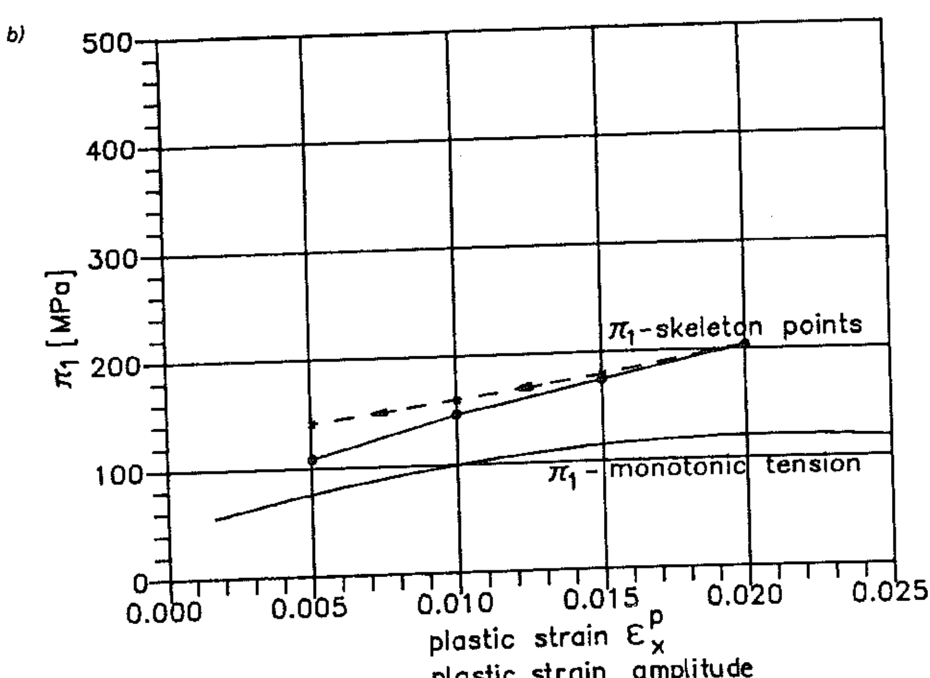
b)
500
400
300
200
100
0
π$_1$ [MPa]
π$_1$ - skeleton points
π$_1$ - monotonic tension
0.000
0.005
0.010
0.015
0.020
0.025
plastic strain ε$_x^p$
plastic strain amplitude

[FIG. 6]

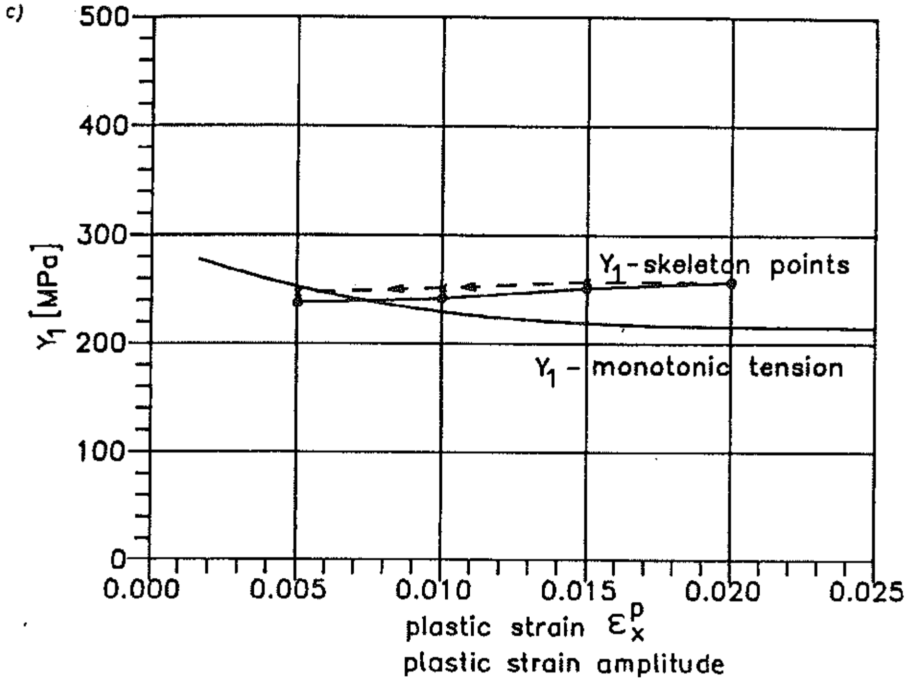

FIG. 6. a) σ skeleton points for increasing strain amplitudes (solid line) and decreasing strain amplitudes (dashed line), b) π_1 skeleton points for increasing strain amplitudes (solid line) and decreasing strain amplitudes (dashed line), c) Y_1 skeleton points for increasing strain amplitudes (solid line) and decreasing strain amplitudes (dashed line).

amplitude $\varepsilon_x^p = \pm 0.015$ are shown in Fig. 7. After hardening caused by plastic prestrain, cyclic relaxation of stresses σ and π_1 (Fig. 7a), but mainly in the prestrain direction, is observed. In the direction opposite to the prestrain, the shapes of the stress-strain and the π_1 curves remain almost unchanged from the very beginning. After several cycles, a steady cycle becomes nearly symmetric. Memory of large uniaxial prestrain was almost erased by cyclic loading with the amplitude mentioned above. Quite symmetric behaviour of Y_1 is observed from the very beginning (Fig. 7b).

When, after such a prestrain ($\varepsilon_x^p = 0.092$), smaller plastic strain amplitude $\varepsilon_x^p = \pm 0.005$ was applied (Fig. 8), even after many cycles the stress and values of π_1 at the prestrained direction do not relax to the corresponding values in the "opposite direction" (Fig. 8a), and steady cycle remains non-symmetric (symmetric behaviour of Y_1 is still observed – Fig. 8b). In such a case, memory of a large uniaxial prestrain cannot be erased by cyclic loading with comparatively small cyclic amplitude and, after such a history, steady state cyclic curve remains unsymmetrical. Such material memory is included in the behaviour of the parameter π_1.

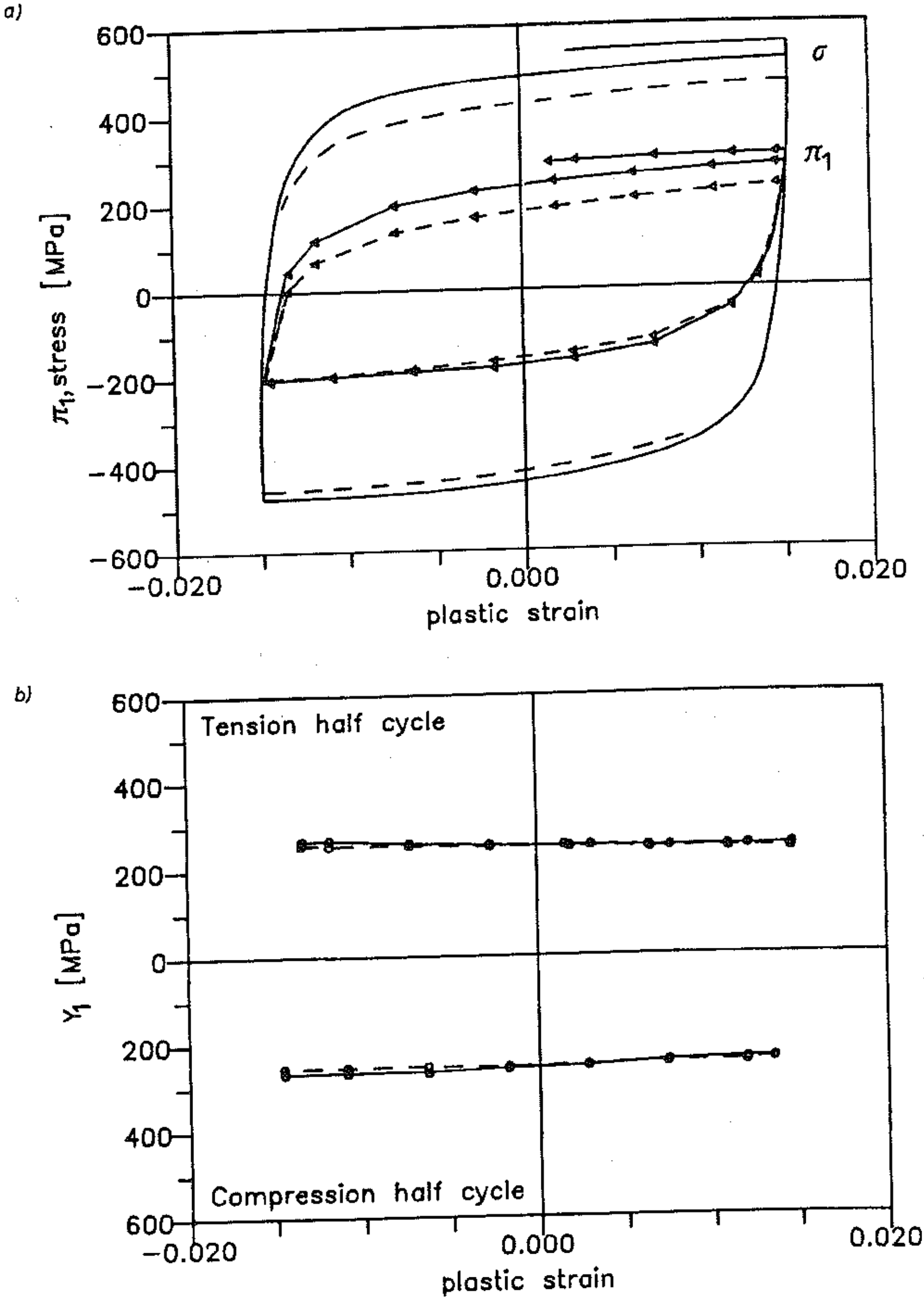

FIG. 7. Cyclic tension-compression loading with $\varepsilon_x^p = \pm 0.015$ strain amplitude after monotonic tension up to $\varepsilon_x^p = 0.092$, Δ – π_1 evolution (kinematic hardening), o – Y_1 evolution (isotropic hardening).

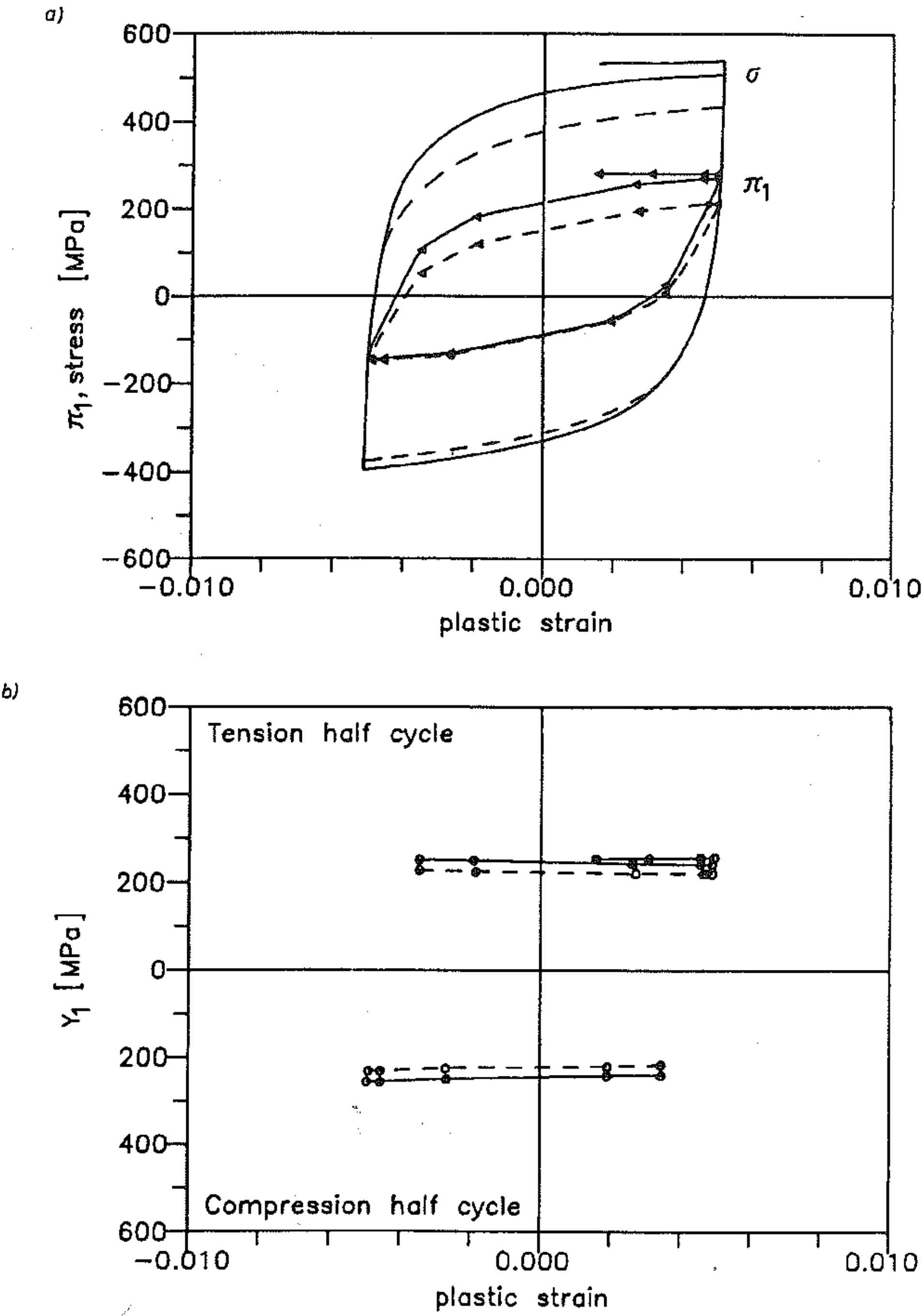

FIG. 8. Cyclic tension-compression loading with $\varepsilon_x^p = \pm 0.005$ strain amplitude after monotonic tension up to $\varepsilon_x^p = 0.092$, Δ – π_1 evolution (kinematic hardening), o – Y_1 evolution (isotropic hardening).

c. Stress-controlled cyclic tension-compression (ratchetting)

The ratchetting phenomenon corresponds to the progressive distortion, cycle-by-cycle, induced by superposition of a primary loading (considered as constant) and a secondary cyclic loading. Under uniaxial conditions, the mean stress σ_m can be considered as the "primary load" and the cyclic stress (amplitude σ_a) as the secondary one. The ratchetting parameters used in this paper

$\sigma_m = (\sigma_1 + \sigma_2)/2$, $\sigma_a = \sigma_{\max} - \sigma_m$, $\delta\varepsilon^p_t$ *(one cycle tension plastic strain)*, $\delta\varepsilon^p_c$ *(one cycle compression plastic strain)*, $\delta\varepsilon^p_r$ *(one cycle ratchetting strain* $\delta\varepsilon^p_r = \delta\varepsilon^p_t + \delta\varepsilon^p_c$*)*, $\delta\varepsilon^{ps}_c$ *(one cycle ratchetting strain at steady state) and ratchetting strain after N cycles* $\varepsilon^p_r = \sum_{i=1}^{i=N} \delta\varepsilon^p_r$

are presented in Fig. 9.

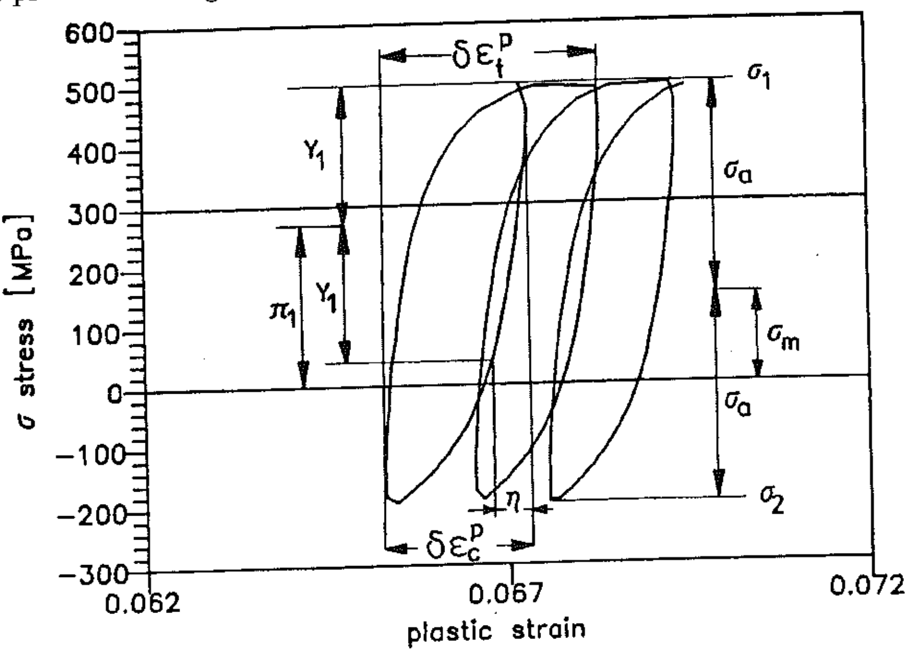

FIG. 9. Main ratchetting parameters.

A typical stress-strain response of 18G2A steel cycled under tension-compression with a positive mean stress $\sigma_m = 150$ MPa and cyclic amplitude $\sigma_a = 350$ MPa is shown in Fig. 10a (AB – monotonic load, a – first 10 cycles, b – last 10 cycles). The induced hystheresis loops never close and, as a result, the recorded strain gradually ratchets in the direction of the mean stress. The ratchetting strain ε^p_r is plotted in Fig. 10b as a function of the number of cycles (N). At the beginning the rate of ratchetting is higher (transition period), and then (as the material hardens) decreases to an approximately constant value (linear decrease) characteristic for the steady state. π_1 increases and Y_1 decreases, reaching almost constant values at the steady state (Fig. 10c).

In Fig. 10d, the values of $|\delta\varepsilon_t^p|$ (one cycle ratchetting tension strain moduli) and $|\delta\varepsilon_c^p|$ (one cycle ratchetting compression strain moduli) are presented as functions of the number of cycles N. The difference between these two values represents one cycle ratchetting strain $\delta\varepsilon_r^p$.

To check the influence of cyclic amplitude and mean stress on the material cyclic behaviour, several (7) sets of experiments were conducted. In every set, the mean stress was kept constant and the amplitude of the cycle was increased step by step. For a chosen amplitude, the cyclic loading was repeated until one cycle ratchetting strain $\delta\varepsilon_r^p$, recorded in the following cycles, becomes either constant (steady state) or zero (shakedown). Then, higher amplitude (cycling amplitude was increased to 20 MPa) was applied and the specimen was cyclically loaded until a new steady state and so on. Results of such an experimental program for mean stress $\sigma_m = 300$ MPa are shown in Fig. 11a as the diagram of ratchetting strain ε_r^p versus the number of cycles. Results of this program, but presented as $|\delta\varepsilon_t^p|$ and $|\delta\varepsilon_c^p|$ one-cycle ratchetting strains versus the number of cycles (N) are shown in Fig. 11b. In the case of no ratchetting behaviour ($\sigma_a = 50$ MPa) $|\delta\varepsilon_t^p|$ and $|\delta\varepsilon_c^p|$ are equal from the beginning, in the case of ratchetting shakedown behaviour ($\sigma_a = 60, 110, 160, 200$ MPa) $|\delta\varepsilon_t^p|$ and $|\delta\varepsilon_c^p|$ values coincide at the steady state, and in the case of ratchetting behaviour their values differ. This was the procedure of determination of the shakedown behaviour.

Similar tests were performed for different mean stress and the data concerning one-cycle ratchetting strain ($\delta\varepsilon_r^{ps}$) at a steady state versus the stress amplitude, are shown in Fig. 12. Three types of material behaviour (depending on σ_m and σ_a) can be distinguished:

I – no ratchetting, II – ratchetting shake-down and III – ratchetting (in Fig. 11b such types of behaviour are distinguished for $\sigma_m = 300$).

The boundary points of such behaviour are presented in Fig. 13, and zones of different material behaviour can be determined in coordinates $\sigma_m - \sigma_a$ (Fig. 13a) and $\sigma_{\max} - \sigma_a$ (Fig. 13b). It is shown that using such data, the map of material cyclic behaviour can be created. It is seen (Fig. 13b) that, in the case of stress-controlled cyclic loading, material cyclic behaviour can be determined provided only two parameters: the virgin material yield value (σ_Y) and the bounding amplitude (σ_{al}) are known. For maximal stress below

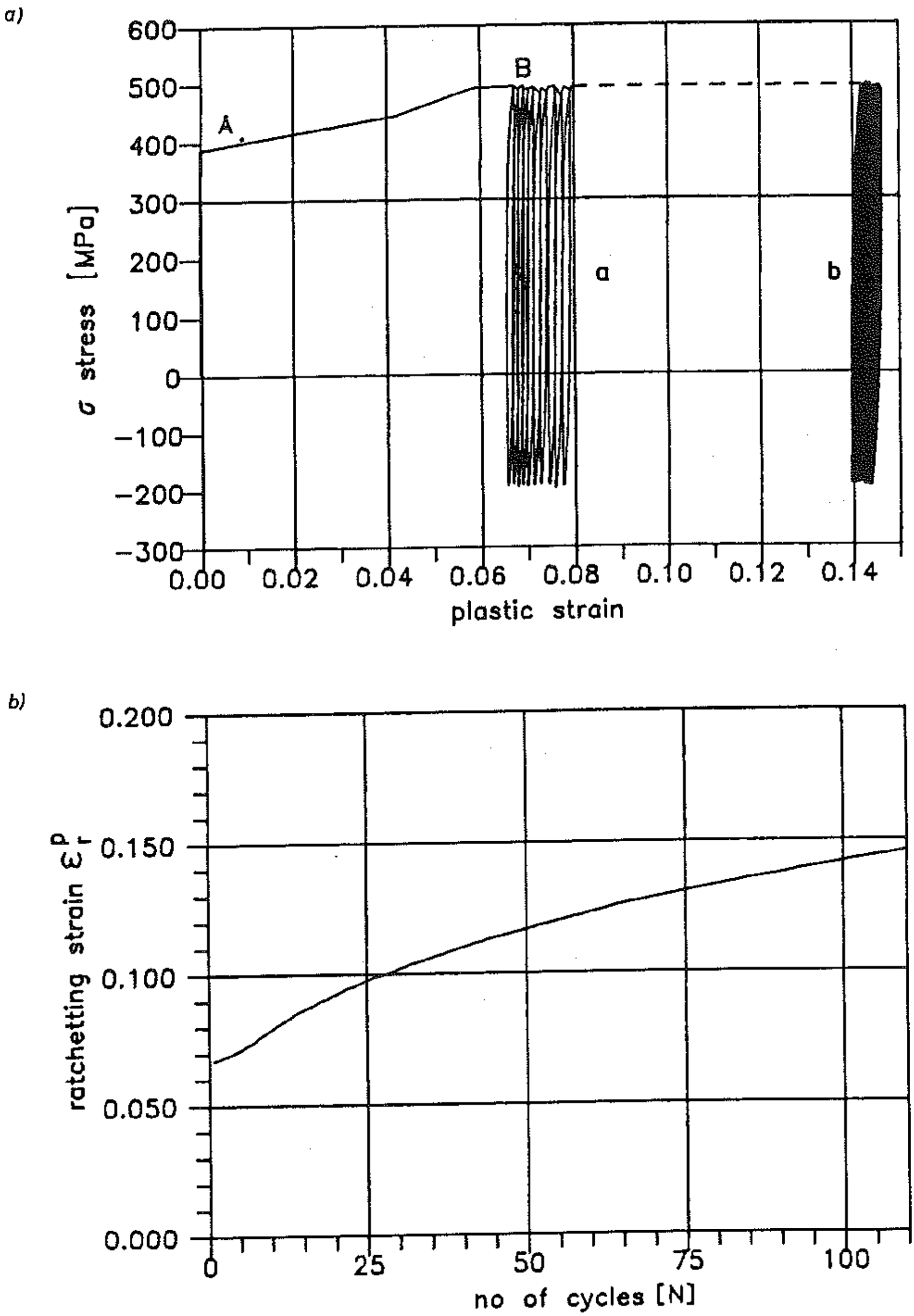
a)
600
500
400
300
200
100
0
−100
−200
−300
0.00
0.02
0.04
0.06
0.08
0.10
0.12
0.14
plastic strain
σ stress [MPa]
A
B
a
b
b)
0.200
0.150
0.100
0.050
0.000
0
25
50
75
100
no of cycles [N]
ratchetting strain ε_r^p

[FIG. 10]

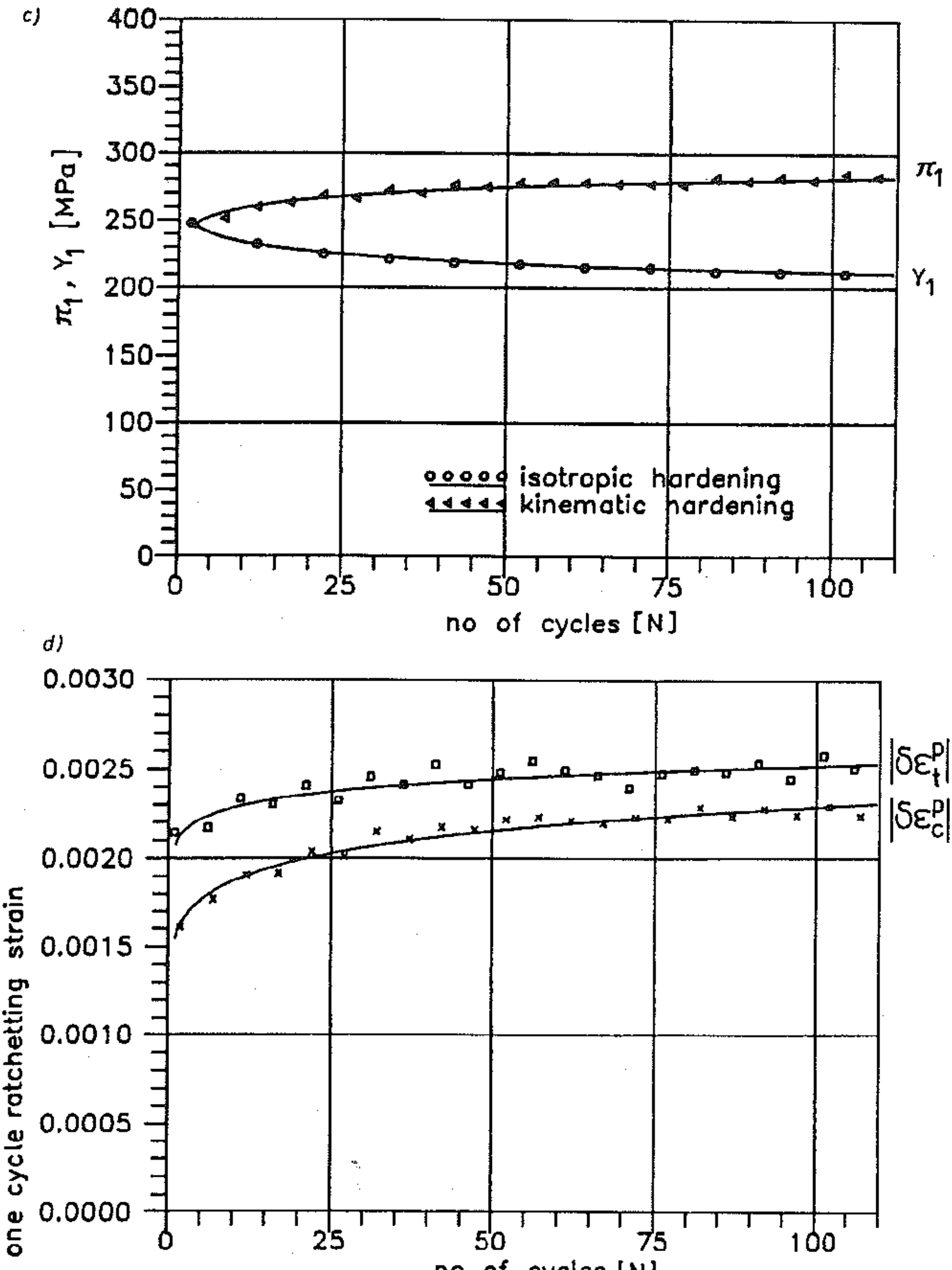

FIG. 10. a) Stress-plastic strain curve for cyclic tension-compression loading ($\sigma_m = 150\,\mathrm{MPa}$, $\sigma_a = 350\,\mathrm{MPa}$), a – first 10 cycles, b – last 10 cycles. b) Ratchetting strain ε_r^p versus the number of cycles for cyclic tension-compression loading ($\sigma_m = 150\,\mathrm{MPa}$, $\sigma_a = 350\,\mathrm{MPa}$). c) π_1 and Y_1 values versus the number of cycles for cyclic tension-compression loading ($\sigma_m = 150\,\mathrm{MPa}$, $\sigma_a = 350\,\mathrm{MPa}$), d) $|\delta\varepsilon_t^p|$ and $|\delta\varepsilon_c^p|$ versus the number of cycles for cyclic tension-compression loading ($\sigma_m = 150\,\mathrm{MPa}$, $\sigma_a = 350\,\mathrm{MPa}$).

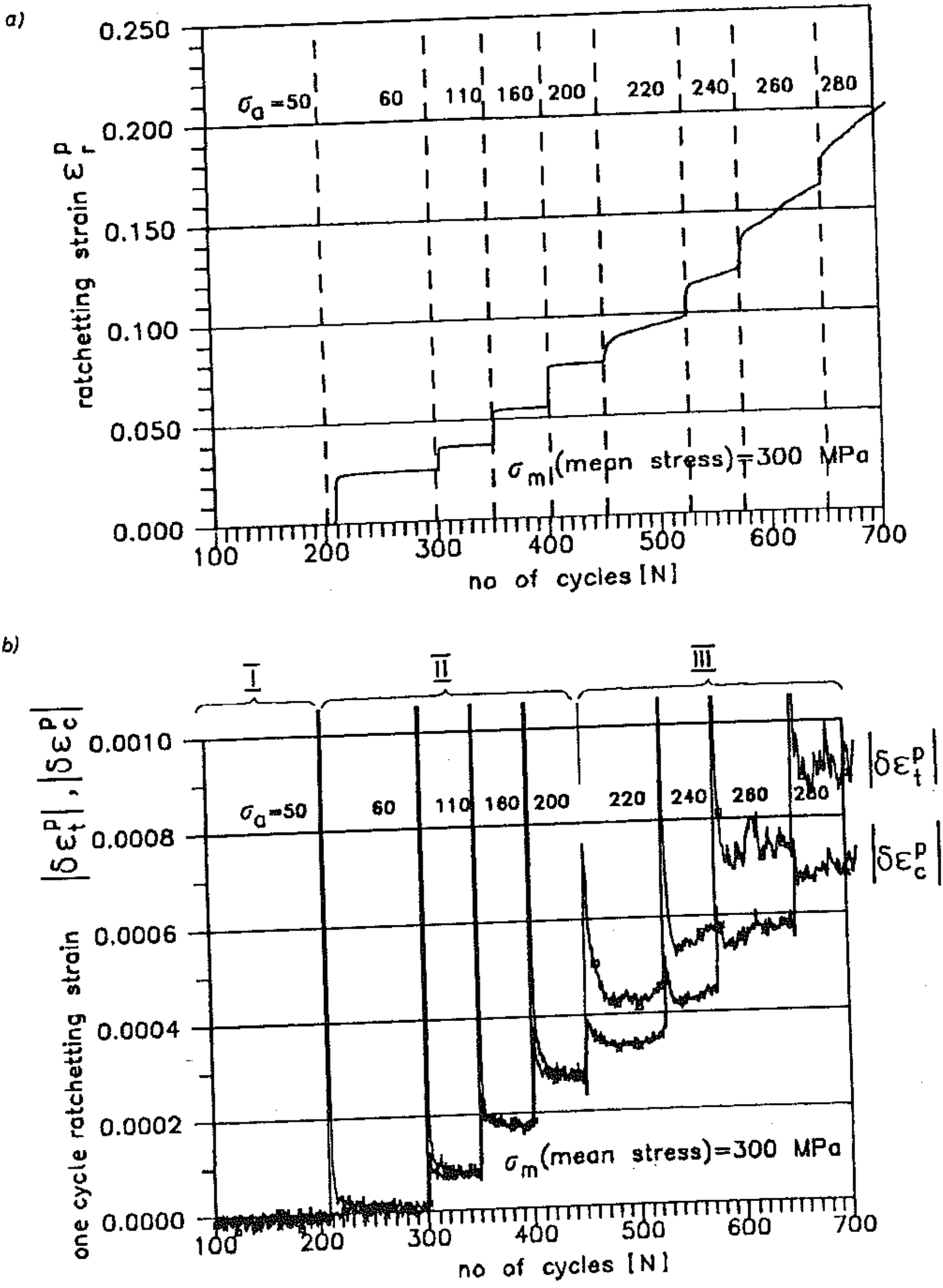

FIG. 11. a) Ratchetting strain ε_r^p versus the number of cycles for cyclic tension-compression loading with varying amplitudes ($\sigma_m = 300\,\mathrm{MPa}$, $\sigma_a = 50 - 280\,\mathrm{MPa}$). b) $|\delta\varepsilon_r^p|$ and $|\delta\varepsilon_c^p|$ one-cycle ratchetting strains versus growing number of cycles (N) for cyclic tension-compression loading with varying amplitudes ($\sigma_m = 300\,\mathrm{MPa}$, $\sigma_a = 50 - 280\,\mathrm{MPa}$).

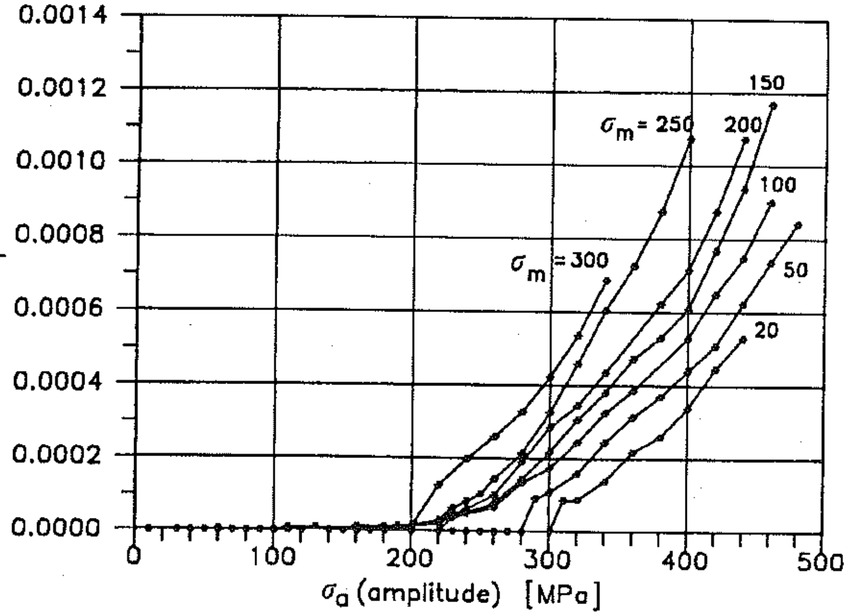

FIG. 12. One-cycle ratchetting steady state strain $\delta\varepsilon_r^{ps}$ versus cyclic amplitude σ_a for cyclic tension-compression loading, with different mean stresses and growing cyclic amplitudes.

the yield limit $\sigma_{\max} < \sigma_Y$ only no-ratchetting behaviour is observed. In the case when $\sigma_{\max} \geq \sigma_Y$, two kinds of behaviour can be expected:

ratchetting for $\sigma_a > \sigma_{al}$ and ratchetting shake-down for $\sigma_a \leq \sigma_{al}$ (except of $\sigma_m = 0$, when ratchetting effect does not occur in any case).

One cycle ratchetting strain at the steady state ($\delta\varepsilon_r^{ps}$) can be described by the following power relation:

$$(3)\qquad \begin{aligned} \delta\varepsilon_r^{ps} &= 0 && \text{for } (\sigma_m + \sigma_a) < \sigma_Y \quad \text{or} \\ & && \text{for } (\sigma_m + \sigma_a) \geq \sigma_Y \quad \text{and} \quad \sigma_a \leq \sigma_{al}, \\ \delta\varepsilon_r^{ps} &= A[(\sigma_a - \sigma_{al})/\sigma_Y]^n && \text{for } (\sigma_m + \sigma_a) \geq \sigma_Y \quad \text{and} \quad \sigma_a > \sigma_{al}, \end{aligned}$$

where $n = 1.56$ and $A = A(\sigma_m/\sigma_Y)$, σ_Y – yield limit (for this material 340 MPa), σ_{al} – limit amplitude (for this material 200 MPa).

Comparison between the experimental and theoretical results calculated this way is shown in Fig. 14 (experimental results – dashed lines, and theoretical results – solid lines), assuming A to take values as shown in Fig. 15 (asterisks $*$ connected by dashed line). This function can be expressed by following relation (Fig. 15 – solid line):

$$(3')\qquad A = 0.0583(\sigma_m/\sigma_Y)[(\sigma_m/\sigma_Y)^4 - 2.539(\sigma_m/\sigma_Y)^3 + 2.487(\sigma_m/\sigma_Y)^2 - 1.108(\sigma_m/\sigma_Y) + 0.24].$$

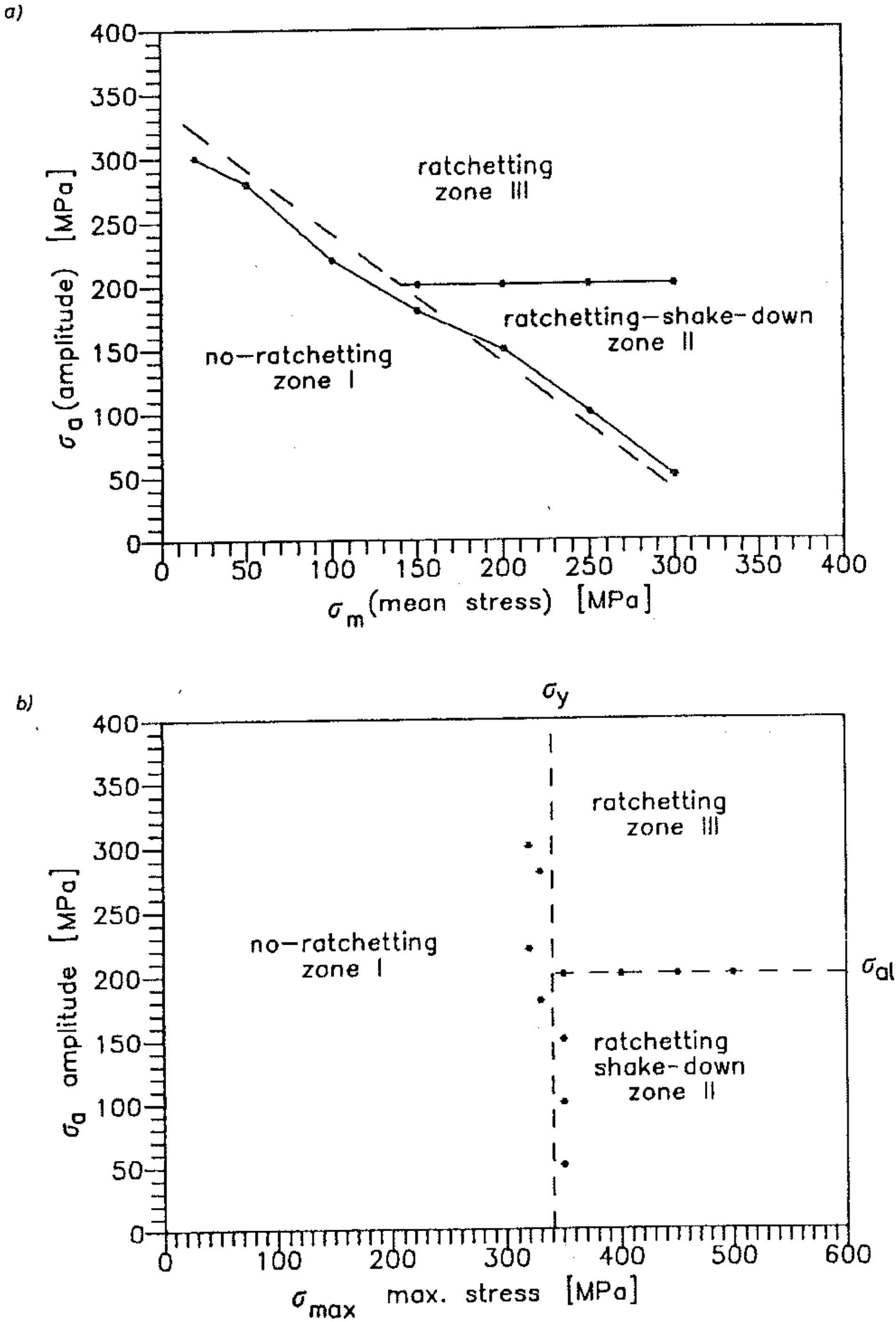

FIG. 13. Cyclic behaviour zones.

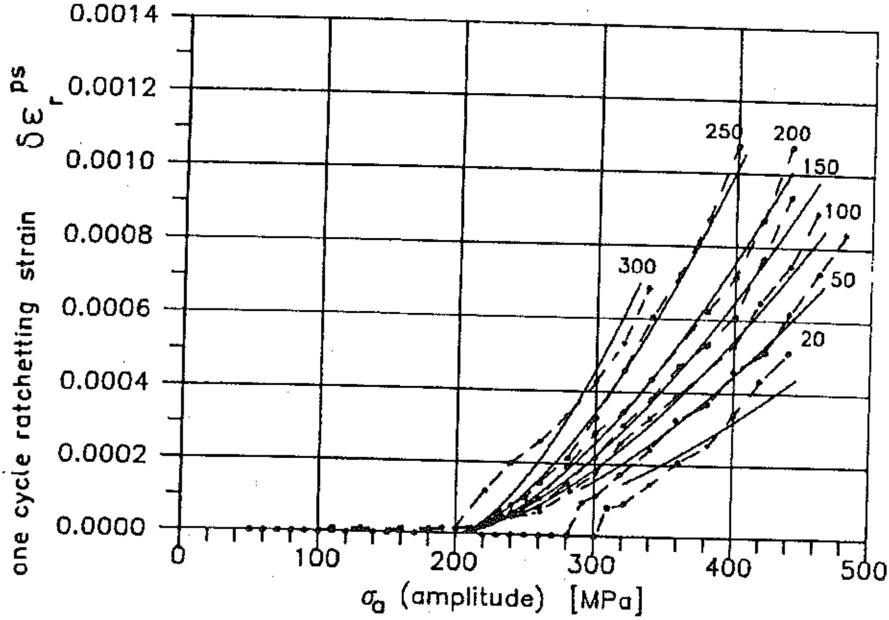

FIG. 14. One-cycle ratchetting steady state strain $\delta\varepsilon_r^{ps}$ versus cyclic amplitude σ_a for cyclic tension-compression loading with different mean stresses, $-*-*-*-*-$ experimental results, —— theoretical prediction.

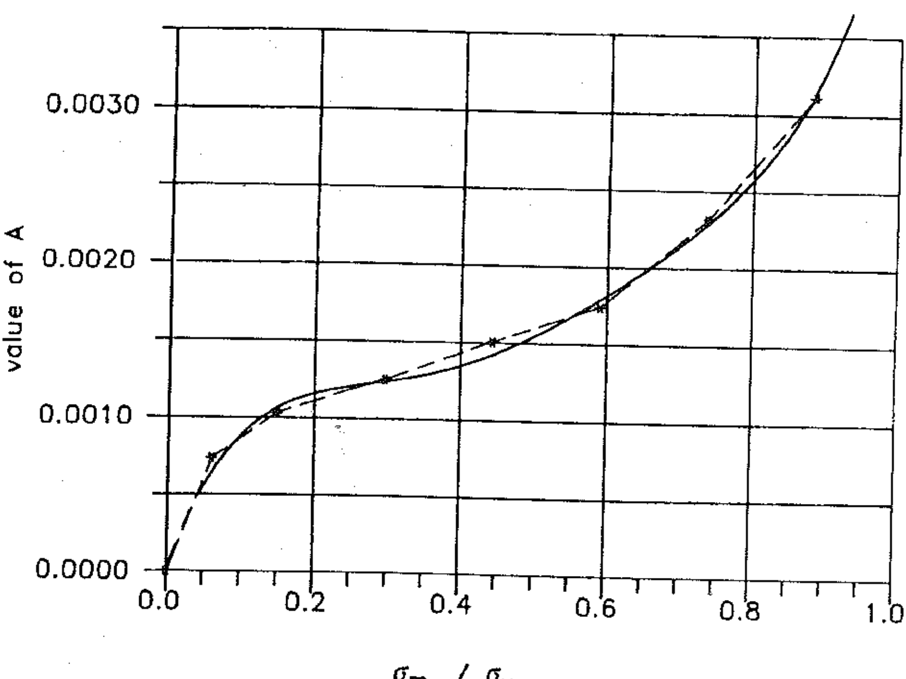

FIG. 15. A values (Eq. (3)), $-*-*-*-*-$ values of A assumed for the theoretical calculation, —— values of A described by Eq. (3′).

The experimental results presented in Fig. 14 are shown in Fig. 16 as the diagram of the one-cycle steady state ratchetting $\delta\varepsilon_r^{ps}$ versus $(\sigma_a - \sigma_{al})/\sigma_Y$.

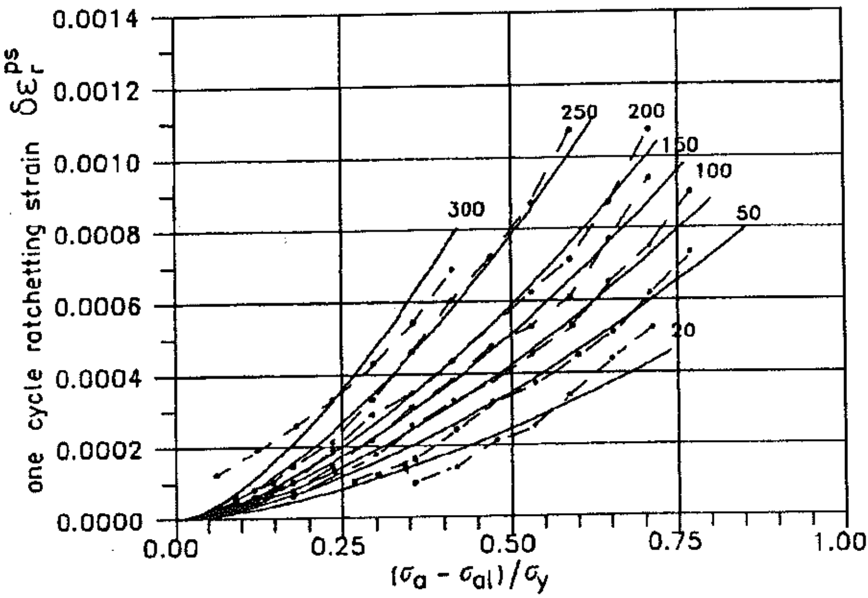

FIG. 16. One-cycle ratchetting steady state strain $\delta\varepsilon_r^{ps}$ versus $(\sigma_a - \sigma_{al})/\sigma_Y$ for cyclic tension-compression loading with different mean stresses, – * – * – * – * – experimental results, —— theoretical prediction.

It was observed that the steady state one-cycle ratchetting $\delta\varepsilon_r^{ps}$ depends on the steady state one-cycle hystheresis loop dimension. It may be expressed by

$$\delta\varepsilon_{rh}^{ps} = (|\delta\varepsilon_t^{ps}| + |\delta\varepsilon_c^{ps}|)/2, \tag{4}$$

where $\delta\varepsilon_t^{ps}$ and $\delta\varepsilon_c^{ps}$ are steady-state one cycle tension and compression plastic strains, respectively.

The results presented in Fig. 14 are shown also in Fig. 17 in new coordinates: one-cycle ratchetting steady state strain $(\delta\varepsilon_r^{ps})$ versus steady state hystheresis loop measure $\delta\varepsilon_{rh}^{ps}$, and compared with the following power relation (solid lines):

$$\delta\varepsilon_r^{ps} = B(\delta\varepsilon_{rh}^{ps})^m, \qquad \text{where} \quad m = 1.56 \quad \text{and} \quad B = B(\sigma_m). \tag{5}$$

It was assumed that B takes the values shown in Fig. 18 (asterisks * connected by dashed line). This function can be expressed by the following relation (Fig. 18 – solid line):

$$B = 7.3(\sigma_m/\sigma_Y)[4(\sigma_m/\sigma_Y)^2 - (\sigma_m/\sigma_Y) + 1]. \tag{5'}$$

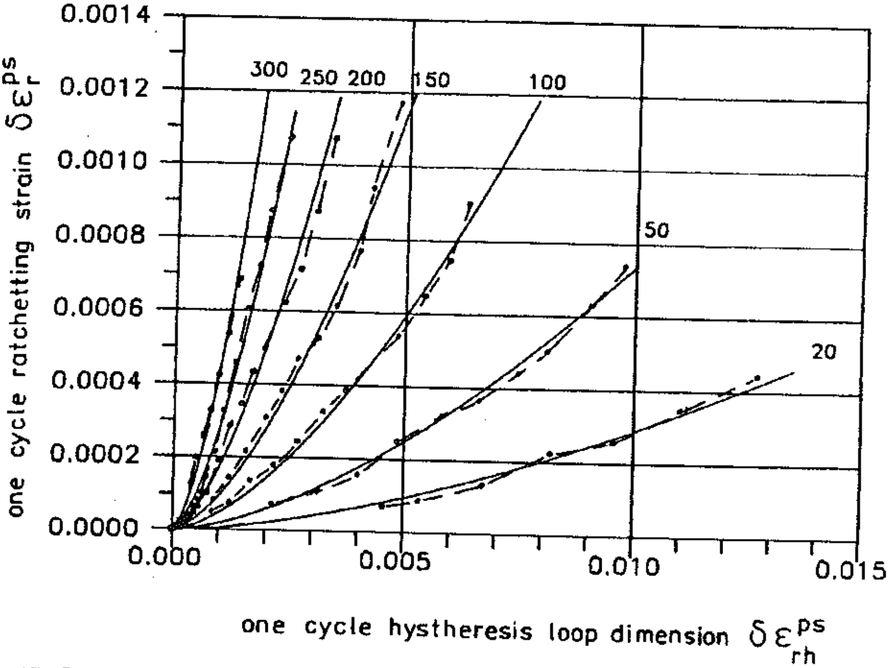

FIG. 17. One-cycle ratchetting steady state strain $\delta\varepsilon_r^{ps}$ versus one-cycle hystheresis loop dimension $\delta\varepsilon_{rh}^{ps}$ for cyclic tension-compression with different mean stresses and growing cyclic amplitudes, $- * - * - * - * -$ experimental results, —— theoretical prediction.

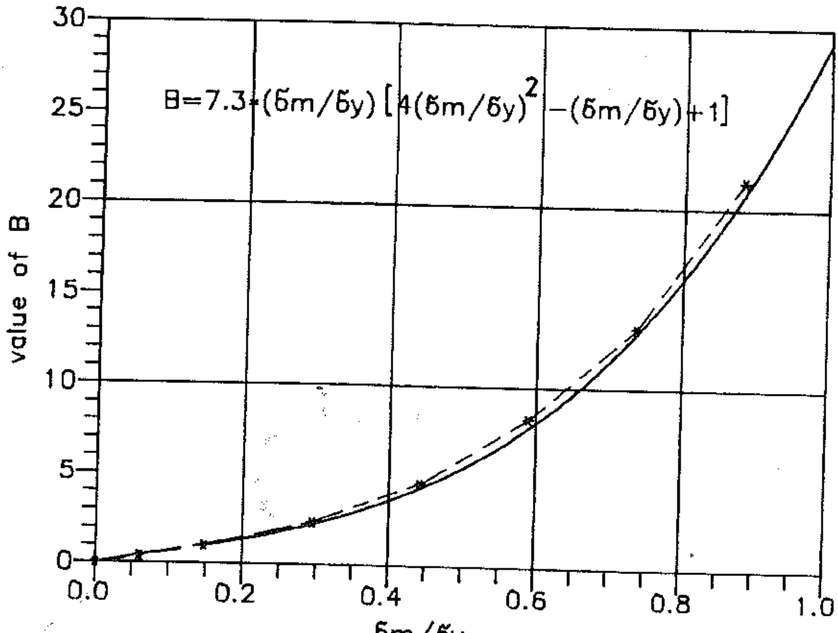

FIG. 18. B values (Eq. (5)), $- * - * - * - * -$ values of A assumed for the theoretical calculation, —— values of A described by Eq. (5′).

The results presented in Fig. 14 were obtained by a step-by-step approach (constant mean stress σ_m and increasing amplitude σ_a) on one specimen. Results for the two following amplitudes, where the first one was applied to virgin specimens (one point – one specimen) are presented in Fig. 19 (asterisks; $a^1 - a^2$; $b^1 - b^2$; ...) and compared with that for step-wise loading (solid line) showing good agreement. It means that cyclic loading with smaller amplitudes has no influence on material behaviour with higher amplitudes and relations (3) and (5) describe the ratchetting behaviour also for virgin specimens.

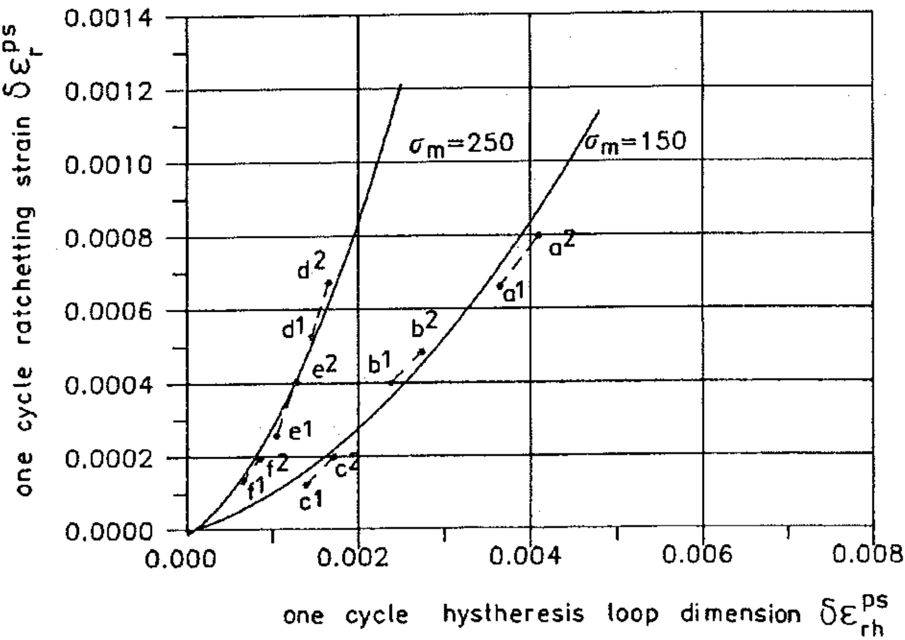

FIG. 19. One-cycle ratchetting steady state strain $\delta\varepsilon_r^{ps}$ versus one-cycle hystheresis loop dimension $\delta\varepsilon_{rh}^{ps}$ for cyclic tension-compression loading with different mean stresses and growing cyclic amplitudes, —— results for stepwise growing amplitudes (Fig. 17), – * – * – * – * – results for virgin specimens.

Experimental results for this same mean stress $\sigma_m = 150$ and 250 MPa (as in Fig. 19), but a different amplitude sequence, is presented in Fig. 20.

The specimen was first loaded (Fig. 20a – $\sigma_m = 150$) by the amplitude represented by point 1 – program a ($\sigma_a = 400$ MPa) – virgin material, and when the steady state was achieved, the cyclic amplitude was increased to the amplitude represented by point 2 ($\sigma_a = 420$ MPa – dashed line). Then, cyclic amplitude was reduced to the same value as in point 1 ($\sigma_a = 400$ MPa), and steady state ratchetting strain rate represented by point 3 (dashed line) was achieved. Then the cyclic amplitude was reduced to $\sigma_a = 380$, 360, 340 a)

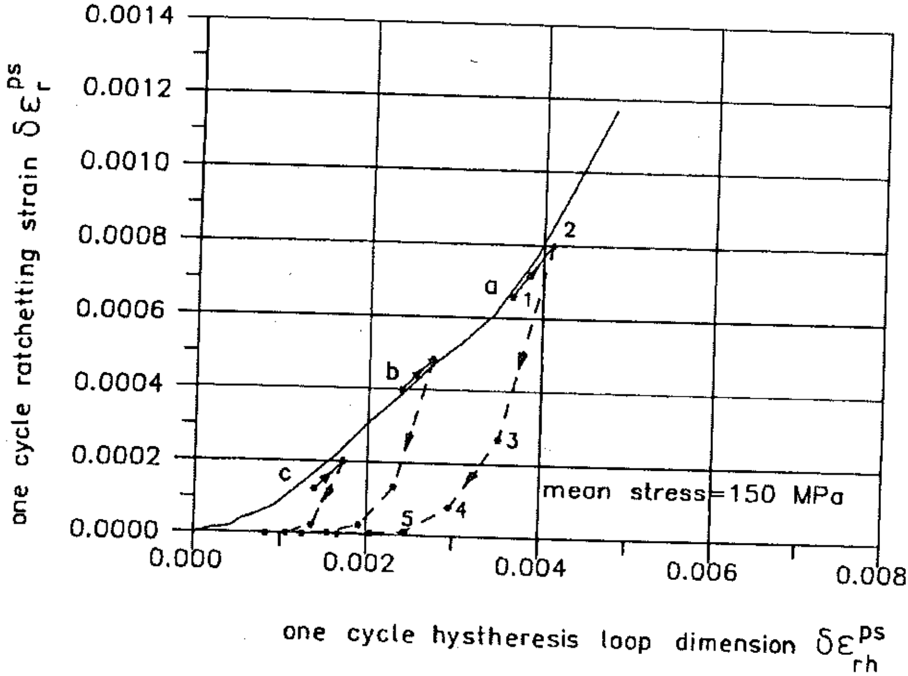
0.0014
0.0012
0.0010
0.0008
0.0006
0.0004
0.0002
0.0000
0.000
0.002
0.004
0.006
0.008
one cycle ratchetting strain $\delta\varepsilon_r^{ps}$
one cycle hystheresis loop dimension $\delta\varepsilon_{rh}^{ps}$
mean stress=150 MPa
a
b
c
1
2
3
4
5

b)

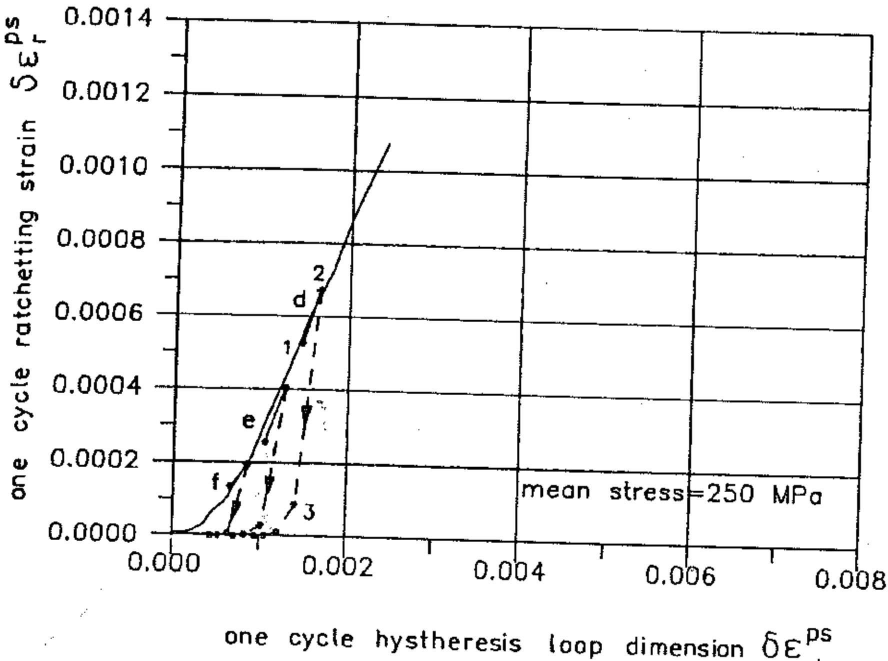
0.0014
0.0012
0.0010
0.0008
0.0006
0.0004
0.0002
0.0000
0.000
0.002
0.004
0.006
0.008
one cycle ratchetting strain $\delta\varepsilon_r^{ps}$
one cycle hystheresis loop dimension $\delta\varepsilon_{rh}^{ps}$
mean stress=250 MPa
d
e
f
1
2
3

[FIG. 20]

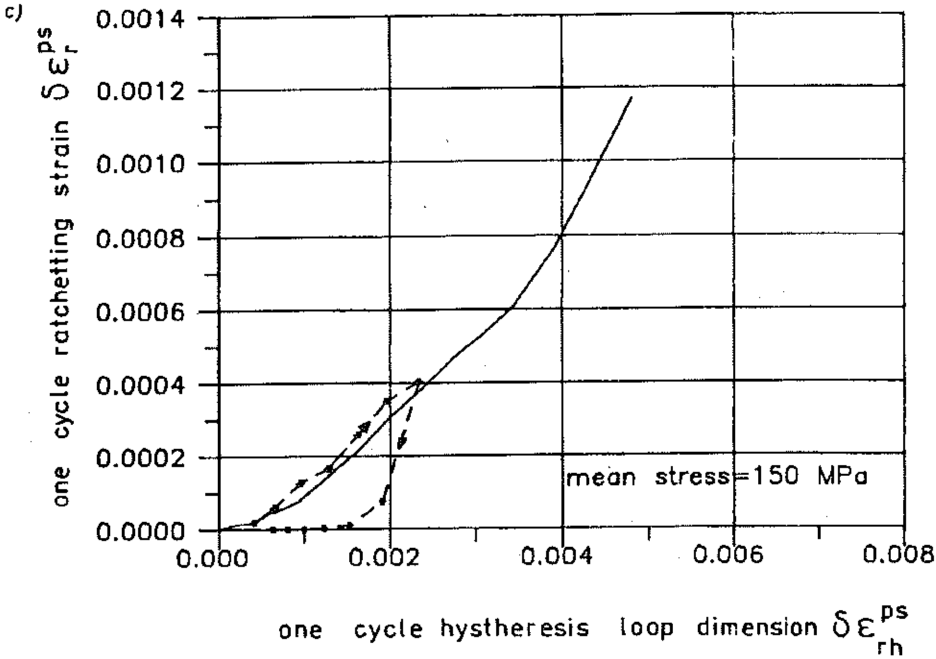

FIG. 20. One-cycle ratchetting steady state strain $\delta\varepsilon_r^{ps}$ versus one-cycle hystheresis loop dimension $\delta\varepsilon_{rh}^{ps}$ for cyclic tension-compression with constant mean stress σ_m and varying cyclic amplitudes σ_a, —— results for stepwise growing amplitudes (Fig. 18).

a) $\sigma_m = 150$ MPa, $- * - * - * -$ results for the following amplitudes: a $\sigma_a = 400; 420; 400; 380; 360; 340; 320$ MPa, b $\sigma_a = 340; 360; 340; 320; 300; 280$ MPa, c $\sigma_a = 280; 300; 280; 260; 240$ MPa.

b) $\sigma_m = 250$ MPa, $- * - * - * -$ results for the following amplitudes: d $\sigma_a = 340; 360; 340; 320; 300; 280$ MPa, e $\sigma_a = 300; 320; 300; 280; 260$ MPa, f $\sigma_a = 260; 280; 260; 240; 220$ MPa.

c) $\sigma_m = 150$ MPa, $- * - * - * -$ results for the following amplitudes: $\sigma_a = 220; 240; 260; 280; 300; 320; 340; 320; 300; 280; 260; 240; 220$ MPa.

and 320 MPa (broken line). Discrepancy between the solid line and the following points 3, 4, 5, etc. (Fig. 20a) indicates the influence of the cyclic loading history with higher amplitudes on the material behaviour under cyclic loading with smaller amplitudes. When the cyclic amplitudes decrease (for the same mean stress value), the resulting one-cycle ratchetting strain at steady state $\delta\varepsilon_r^{ps}$ is much lower than that for the virgin material (compare points 1 and 3 – the ratchetting strain differ by more than 100%).

Then, similar experiments were repeated for the same mean stress ($\sigma_m = 150$ MPa) but different amplitude history:

$$b \quad \sigma_m = 150\,\text{MPa}, \quad \sigma_a = 340; 360; 340; 320; 300; 280\,\text{MPa},$$
$$c \quad \sigma_m = 150\,\text{MPa}, \quad \sigma_a = 280; 300; 280; 260; 240\,\text{MPa}.$$

In Fig. 20b and Fig. 20c are shown the results of similar experiments, but for the following loading histories:

Fig. 20b

d $\sigma_m = 250$ MPa, $\sigma_a = 340; 360; 340; 320; 300; 280$ MPa,

e $\sigma_m = 250$ MPa, $\sigma_a = 300; 320; 300; 280; 260$ MPa,

f $\sigma_m = 250$ MPa, $\sigma_a = 260; 280; 260; 240; 220$ MPa;

Fig. 20c

$\sigma_m = 150$ MPa, $\sigma_a = 220; 240; 260; 280; 300; 320; 340; 220$ MPa.

They show similar memory effect.

All the experiments, mentioned above, show strong memory effect of cyclic loading with higher amplitudes on the material behaviour under cyclic loading with smaller amplitude. This memory effect is manifested by a substantial reduction of the ratchetting strain rate.

4. Conclusions

1. In the case of monotonic loading the parameters π_1 and Y_1 change simultaneously. The values of Y_1 saturate at plastic strains $\varepsilon_x^p \approx 0.1$, and further material hardening is caused only by increasing π_1. The yield knee is formed as a result of two processes: increase of the parameter π_1 (kinematic hardening) and decrease (isotropic hardening) of the parameter Y_1.

2. The general shape of the π_1 path during cyclic loading (strain-controlled and stress-controlled) is established during the first full cycle, and then it changes only slightly to reach a stabilized loop. The shape of this loop is similar to that of the stress-strain loop ($Y_1 = \text{const}$).

3. Influence of the cyclic history with higher strain amplitudes on the subsequent cyclic behaviour with smaller amplitudes (memory of maximum prestress) is observed in the π_1 parameter behaviour. No influence on the values of Y_1 is observed.

4. Proportional cyclic loading after plastic prestrain leads to relaxation of π_1 in the prestrain direction. In the opposite direction the shape of π_1 curve remains almost constant right from the very beginning of the cyclic program. Value of Y_1 relaxes symmetrically. Memory of large uniaxial prestrain can not be erased by comparatively small cyclic loading and, after such a history, steady state cyclic curve remains unsymmetrical (Fig. 8). Such material memory is included in the behaviour of the parameter π_1. When the cyclic loading is applied with comparatively high amplitudes, such memory can be almost erased (Fig. 7).

5. In stress-controlled cyclic limits, material cyclic behaviour described as ratchetting, ratchetting shake-down or no-ratchetting, can be described only in terms of the virgin material yield value and the bounding amplitude. Knowing only these two data one can define the cyclic loading parameters relating the material behaviour to these three zones.

6. One cycle ratchetting strain at the steady state can be described by a power relation (Eqs. (3) and (5)).

7. The material shows a strong memory of the cyclic history with higher amplitudes on the subsequent cyclic behaviour (ratchetting) with smaller amplitudes.

Acknowledgments

The authors acknowledge support of Polish Committee for Scientific Research under Project 3 P 404 031 04.

References

1. Th. Lehmann, B. Raniecki and W. Trąmpczyński, *The Bauschinger effect in cyclic plasticity*, Arch. Mech., **37**, 6, pp. 643–659, 1985.
2. W. Trąmpczyński, *On a simple experimental technique for the yield surface determination*, Bull. Acad. Polon. Sci., Série Sci. Tech., **37**, 7-12, pp. 407–418, 1989.
3. R. Landgraf, J. Morrow and T. Endo, *Determination of cyclic stress-strain curve*, J. Materials, 4, 176, 1969.
4. H. Jhansale, *A new parameter for the hysteresis stress-strain behavior of metals*, ASME J. Engng. Materials and Technology, 97, 33, 1975.
5. M. Śliwowski, *Behavior of stress-strain diagrams for cyclic loading*, Bull. Acad. Polon Sci., Série Sci. Tech., **27**, 115–123, 1979.
6. Y. Ohashi, M. Kawai and T. Kaito, *Inelastic behavior of type 316 stainless steel*, J. Engng. Mat. Techn., ASME, 111, 278–285, 1985.
7. A. Benallal and D. Marquis, *An experimental investigation of cyclic hardening of 316 stainless steel under complex multiaxial loadings*, Trans. of 9th SMIRT Conf., Vol. L, 345–356, 1987.
8. M. Ohnami, M. Sakane and S. Nishino, *Cyclic behavior of type 304 stainless steel in biaxial stress states at elevated temperatures*, Int. J. Plasticity, 4, 77–89, 1988.
9. H. Ishikawa and K. Sasaki, *Stress strain relations of SUS304 stainless steel after cyclic preloading*, J. Engng. Mat. and Techn., vol. III, 417–423, 1989.
10. T. Hassan and S. Kyriakides, *Ratcheting in cyclic plasticity, Part I. Uniaxial behavior*, Int. J. Plasticity, 8, 91–116, 1992.
11. T. Hassan, E. Corona and S. Kyriakides, *Ratcheting in cyclic plasticity, Part II. Multiaxial behavior*, Int. J. Plasticity, 8, 117–146, 1992.
12. Z. Mróz, *On generalized kinematic hardening rule with memory of maximal prestress*, J. Mech. Appl., 5, 242–260, 1981.

13. Y. DAFALIAS, *A novel bounding surface constitutive law for the monotonic and cyclic hardening response of metals*, 6th SMIRT Conference, 1981.

14. N. OHNO, *A constitutive model of cyclic plasticity with a nonhardening strain region*, J. Appl. Mech, 49, 721–727, 1982.

15. TH. LEHMANN, *General frame for the definition of constitutive laws for large non-isothermic elastic-plastic and elastic-visco-plastic deformation*, The Constitutive Law in Thermoplasticity, CISM, 1984.

16. Y. DAFALIAS, *Modelling cyclic plasticity. Simplicity versus sophistication*, Mechanics of Engineering Materials, C. DESAI and R. GALLAGHER [Eds.], John Willey and Sons, New York, p. 153, 1984.

17. K. VALANIS and C. LEE, *Endochronic plasticity. Physical basis and applications*, Mechanics of Engineering Materials, C. DESAI and R. GALLAGHER [Eds.], John Willey and Sons, New York, p. 591, 1984.

18. D.L. MCDOWELL, *An experimental study of the structure of constitutive equations for non-proportional cyclic plasticity*, ASME J. Engng. Mat. Techn., **107**, 307–315, 1985.

19. J. CHABOCHE, *Time independent constitutive theories for cyclic plasticity*, Int. J. Plasticity, 2, 149, 1986.

20. N. OHNO and Y. KACHI, *A constitutive model of cyclic plasticity for non-linear hardening materials*, J. Appl. Mech., **53**, 395–403, 1986.

21. H. ISHIKAWA and K. SASAKI, *Constitutive modelling of cyclic plasticity considering induced anisotropy*, Constitutive Laws for Engineering Materials, C.S. DESAI *et al.* [Eds.], Elsevier, pp. 581–583, 1987.

22. D.MC. DOWELL, *Simple experimentally motivated cyclic plasticity model*, ASCE J. Engng. Mech., 113, 378, 1987.

23. J. CHABOCHE and D. NOUAILHAS, *Constitutive modelling of ratchetting effects. Part I. Experimental facts and properties of classical models*, ASME J. Engng. Material and Technology, 111, 384, 1989.

24. J. CHABOCHE and D. NOUAILHAS, *Constitutive modelling of ratchetting effects. Part II. Possibilities of some additional kinematic rules*, ASME J. Engng. Material and Technology, 111, 384, 1989.

25. F. ELLYIN and Z. XIA, *A rate-independent constitutive model for transient non-proportional loading*, J. Mech. Phys. Solids, **37**, 1, pp. 71–91, 1989.

26. N. OHNO, *Recent topics in constitutive modelling of cyclic plasticity and viscoplasticity*, ASME Appl. Mech. Revs., **43**, 11, 283–295, 1990.

27. W. TRĄMPCZYŃSKI and Z. MRÓZ, *Anisotropic hardening model and its application to cyclic loading*, [in:] Anisotropy and Localisation of Plastic Deformation, Proc. of Plasticity 91, J.P. BOEHLER and A.S. KHAN [Eds.], Elsevier Applied Science, 1991.

28. W. TRĄMPCZYŃSKI, *The experimental verification of the evolution of kinematic and isotropic hardening in cyclic plasticity*, J. Mech. Phys. Solids, **36**, 4, pp. 417–441, 1988.

POLISH ACADEMY OF SCIENCES
INSTITUTE OF FUNDAMENTAL TECHNOLOGICAL RESEARCH, WARSZAWA.

Received October 26, 1994.